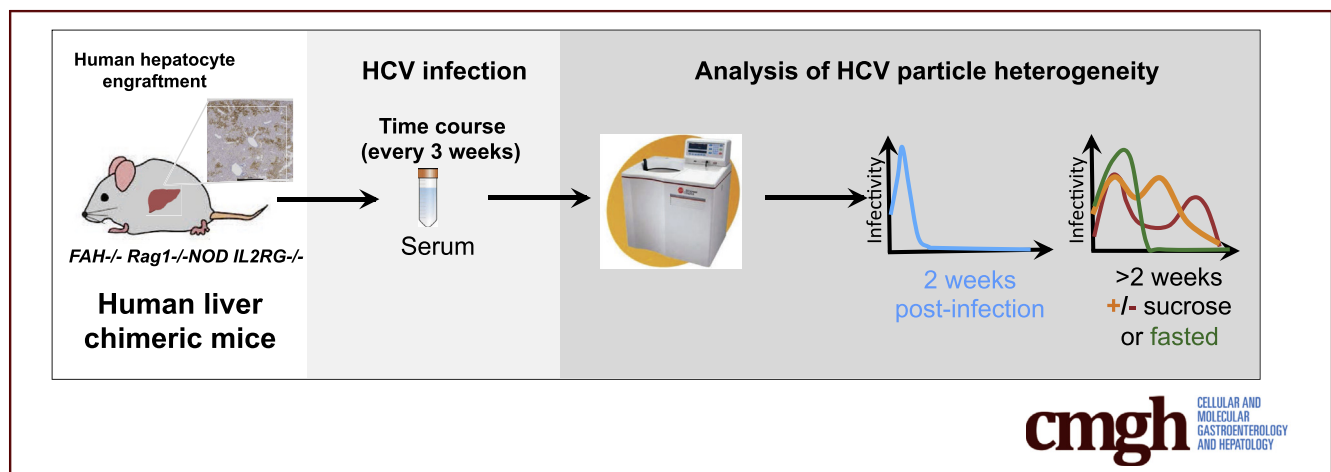


## ORIGINAL RESEARCH

Analysis of Hepatitis C Virus Particle Heterogeneity  
in Immunodeficient Human Liver Chimeric *fah*<sup>-/-</sup> Mice

Ursula Andreo,<sup>1</sup> Ype P. de Jong,<sup>1,2</sup> Margaret A. Scull,<sup>1</sup> Jing W. Xiao,<sup>1</sup> Koen Vercauteren,<sup>1</sup> Corrine Quirk,<sup>1</sup> Michiel C. Mommersteeg,<sup>1</sup> Sonia Bergaya,<sup>3</sup> Arjun Menon,<sup>3</sup> Edward A. Fisher,<sup>3</sup> and Charles M. Rice<sup>1</sup>

<sup>1</sup>Center for the Study of Hepatitis C, The Rockefeller University, New York, New York; <sup>2</sup>Division of Gastroenterology and Hepatology, Center for the Study of Hepatitis C, Weill Cornell Medical College, New York, New York; <sup>3</sup>Division of Cardiology, Department of Medicine, New York University Langone Medical Center, New York, New York



## SUMMARY

Our study describes how the biophysical properties of the hepatitis C virus evolve over the course of infection using the human liver chimeric FAH<sup>-/-</sup> mouse model and suggests that metabolic changes impact hepatitis C virus biophysical properties.

**BACKGROUND & AIMS:** Hepatitis C virus (HCV) is a leading cause of chronic liver diseases and the most common indication for liver transplantation in the United States. HCV particles in the blood of infected patients are characterized by heterogeneous buoyant densities, likely owing to HCV association with lipoproteins. However, clinical isolates are not infectious in vitro and the relative infectivity of the particles with respect to their buoyant density therefore cannot be determined, pointing to the need for better in vivo model systems.

**METHODS:** To analyze the evolution of the buoyant density of in vivo-derived infectious HCV particles over time, we infected immunodeficient human liver chimeric fumaryl acetoacetate hydrolase<sup>-/-</sup> mice with J6/JFH1 and performed ultracentrifugation of infectious mouse sera on isopicnic

iodoxanol gradients. We also evaluated the impact of a high sucrose diet, which has been shown to increase very-low-density lipoprotein secretion by the liver in rodents, on lipoprotein and HCV particle characteristics.

**RESULTS:** Similar to the severe combined immunodeficiency disease/Albumin-urokinase plasminogen activator human liver chimeric mouse model, density fractionation of infectious mouse serum showed higher infectivity in the low-density fractions early after infection. However, over the course of the infection, viral particle heterogeneity increased and the overall in vitro infectivity diminished without loss of the human liver graft over time. In mice provided with a sucrose-rich diet we observed a minor shift in HCV infectivity toward lower density that correlated with a redistribution of triglycerides and cholesterol among lipoproteins.

**CONCLUSIONS:** Our work indicates that the heterogeneity in buoyant density of infectious HCV particles evolves over the course of infection and can be influenced by diet. (*Cell Mol Gastroenterol Hepatol* 2017;4:405–417; <http://dx.doi.org/10.1016/j.jcmgh.2017.07.002>)

**Keywords:** HCV; Lipoprotein; Mouse Model; Human Liver Chimeric Mice.

See editorial on page 443.

Between 130 and 170 million people are chronically infected with hepatitis C virus (HCV) worldwide, putting them at risk for chronic liver disease including steatosis, cirrhosis, and hepatocellular carcinoma.<sup>1</sup> Even with the recent approval of highly effective treatments, HCV remains the primary indication for liver transplantation in the United States and continues to pose a major public health burden. HCV perturbs lipid metabolism, causing liver pathology and potentially contributing to other etiologies including higher risk of cardiovascular diseases,<sup>2,3</sup> the leading cause of death globally. It remains to be determined if the new HCV treatments can revert this phenotype.

HCV is a positive-strand RNA virus that belongs to the *Flaviviridae* family. HCV entry, replication, and assembly are linked closely to host lipid and lipoprotein metabolism.<sup>4–6</sup> It now is understood that the low density and high infectivity of these particles are the result of HCV association with the very-low-density lipoprotein (VLDL) secretion pathway leading to the formation of a lipoviroparticle (LVPs).<sup>7</sup>

Lipoproteins are macromolecular complexes that allow the transport of lipids in the bloodstream. Lipoproteins are composed of a monolayer of phospholipids, in which apolipoproteins are associated. The core of the particle contains cholesterol esters and triglycerides. Lipoprotein subclasses are differentiated by size and buoyant density depending on their triglyceride and cholesterol content. High-density lipoproteins (HDLs) are small dense lipoproteins that are responsible for the transport of cholesterol from peripheral tissues back to the liver in a process called *reverse cholesterol transport*. VLDL are secreted by hepatocytes to mainly transport triglycerides from the liver to extrahepatic tissues. They are transformed in the circulation to intermediate-density lipoprotein and low-density lipoprotein (LDL) after triglyceride hydrolysis by lipoprotein lipase.<sup>8,9</sup>


Despite numerous reports, the precise details of how HCV and host lipoproteins interact, as well as the exact structure of the resulting LVP, remain unknown.<sup>6</sup> Early electron microscopic analyses of patient-derived particles recovered from low-density fractions showed virions with a diameter of 60–70 nm, with immunoreactive viral envelope glycoproteins E1 and E2<sup>10</sup>; viral particles of similar density (<1.1 g/mL) from infected chimpanzees are highly infectious.<sup>11</sup> Recent work from Catanese et al<sup>12</sup> reported that cell culture-derived HCV (HCVcc) particles also are heterogeneous, ranging from 40 to 100 nm. Further biochemical characterization of patient-derived HCC and HCVcc particles confirmed the presence of several apolipoproteins (apos) such as apoB, apoC1, as well as apoE.<sup>13</sup> Besides enhancing infectivity, assembly of lipoprotein-associated viral particles also may provide a means of viral escape from potentially neutralizing antibodies by masking viral epitopes in a lipoprotein coat.<sup>14</sup> Several studies have indicated that apoE is required for HCV infectivity and is part of the LVP.<sup>15–18</sup> Interestingly, a recent study showed that apolipoprotein amphipathic  $\alpha$ -helices were sufficient to promote HCV particle assembly in cell culture.<sup>19</sup> Other important factors for VLDL lipoprotein

assembly, such as the microsomal transfer protein,<sup>16</sup> apoB,<sup>16</sup> and DGAT1<sup>20</sup> have been proposed to play a role in HCV assembly. Even though these in vitro studies have shed some light on the role of lipoproteins in HCV assembly, Huh-7-derived human hepatoma cell lines used to produce HCV particles secrete only partially lipidated immature VLDL,<sup>21</sup> limiting their utility in characterizing the density heterogeneity, composition, and evolution of HCV virions.

There are no fully immunocompetent small-animal models for efficient HCV infection, but several immunodeficient murine xenograft models exist to study HCV infection in vivo. In 1 such model, the severe combined immunodeficiency disease (SCID)/Albumin-urokinase plasminogen activator mouse, in vivo-derived HCV RNA was enriched in the lower density fractions and of higher specific infectivity than in vitro-derived HCV. However, titers were too low to be determined for each fraction.<sup>22</sup> Moreover, the degree of humanization of the lipoprotein profiles in SCID/Alb-uPA liver chimeric mice is reported to correlate with infection success.<sup>23</sup>

In the present study, to analyze the biophysical properties of HCV particles over time, we used an alternative human liver chimeric mouse model that is based on the absence of the tyrosine catabolic enzyme fumaryl acetoacetate hydrolase (*FAH*)<sup>24</sup> on the immunodeficient nod rag  $\gamma$  (NRG) mouse background<sup>25</sup> (designated FNRG mice). FNRG mice infected with J6/JFH1 constitute a suitable model to analyze the buoyant density distribution of infectious HCV particles in a gradient and monitor their evolution over time, as well as establish the susceptibility of the infectious particles in vivo to natural challenges such as feeding and fasting. After infecting these mice with J6/JFH1 and performing an initial analysis of the density of infectious HCV particles, we subjected these mice to a 10% sucrose diet to increase the production of fully lipidated VLDL, and analyzed the HCV virus distribution on a gradient after feeding or fasting. Overall, data in the FNRG mouse model yielded HCV particles of low density and higher infectivity early after infection, supporting previous results in the SCID/Alb-uPA model. However, over the course of the infection, the viral particle density became more heterogeneous with a decreased population of particles of low density, and the overall in vitro infectivity diminished. We further show that a high sucrose diet and a fed vs fasted state affect the buoyant density distribution of HCV particles.

**Abbreviations used in this paper:** Alb-uPA, Albumin-urokinase plasminogen activator; apo, apolipoprotein; CETP, cholesterol ester transfer protein; FAH, fumaryl acetoacetate hydrolase; FNRG, absence of fumaryl acetoacetate hydrolase on an immunodeficient NOD Rag gamma IL2 deficient mouse background; FPLC, fast-performance liquid chromatography; HCV, hepatitis C virus; HCVcc, cell culture-derived hepatitis C virus; HDL, high-density lipoprotein; LVP, lipoviroparticle; NRG, nod rag  $\gamma$ ; NTBC, nitisinone; PBS, phosphate-buffered saline; SCID, severe combined immunodeficiency disease; VLDL, very low density lipoprotein.

 Most current article

© 2017 The Authors. Published by Elsevier Inc. on behalf of the AGA Institute. This is an open access article under the CC BY-NC-ND license (<http://creativecommons.org/licenses/by-nc-nd/4.0/>).

2352-345X

<http://dx.doi.org/10.1016/j.jcmgh.2017.07.002>

## Materials and Methods

### Cell Culture

Huh-7.5 cells<sup>26</sup> were propagated in Dulbecco's modified Eagle medium (Invitrogen, Carlsbad, CA) containing 5% heat-inactivated fetal bovine serum (HyClone; Thermo Scientific, Waltham, MA) and 0.1 mmol/L nonessential amino acids (Invitrogen, Life Technologies, Carlsbad, CA). All cells were maintained at 37°C with humidified 5% CO<sub>2</sub>.

### Human Liver Chimeric Mice

Mice with a targeted disruption in the fumaryl acetoacetate hydrolase gene (*fah*<sup>-/-</sup>)<sup>27</sup> were provided by Markus Grompe from Oregon Health and Science University and crossed for 13 generations onto the NOD *rag1*<sup>-/-</sup> *il2rg*<sup>null</sup> background as described.<sup>25</sup> Resulting *fah*<sup>-/-</sup> NOD *rag1*<sup>-/-</sup> *il2rg*<sup>null</sup> (FNRG) mice were maintained on nitisinone (NTBC; Yecuris, Tualatin, OR). FNRG mice older than 6 weeks of age were transplanted with 1 × 10<sup>6</sup> cryopreserved human hepatocytes purchased from Celsis (Charles River, Chicago, IL). During hepatocyte engraftment mice were cycled off the drug NTBC on the basis of weight loss and overall health. During the infection experiment mice were cycled off NTBC for 2 weeks and on NTBC for 3–5 days, and serum samples were harvested on the last day off NTBC. All animal work was performed at the Rockefeller University in accordance with the National Institutes of Health Guide for the Care and Use of Laboratory Animals and approved by the Rockefeller University Institutional Animal Care and Use Committee (protocol 12536).

### HCV Plasmid Constructs and Generation of HCVcc Inocula

J6/JFH-1 is an intragenotypic recombinant genotype 2a virus containing J6 sequences from core to NS2.<sup>28</sup> HCVcc stocks were prepared by electroporation of in vitro-transcribed viral RNA into Huh-7.5 cells. Virus was collected in 5% fetal bovine serum, and titers were determined by limiting dilution assay, as described previously.<sup>28</sup> The inoculum was passaged at least 3 times in mice to adapt the virus further to the FNRG mouse model and the mice used for this experiment were infected with 2.04 × 10<sup>5</sup> RNA copies. A large unique stock of mouse-passaged J6/JFH1 could not be generated. Previous experiences with the H77 isolate showed that repeated freezing and thawing reduced the titers considerably. We thus pooled different aliquots of mouse-passaged samples to infect the cohort of mice. An example of the difference in buoyant density profiles of the cell culture-derived and mouse-passaged J6/JFH1 is shown in Figure 1.

### Triglycerides and Cholesterol Measurement

A total of 10 μL of serum or 100 μL of fast-performance liquid chromatography (FPLC) fraction was used for triglyceride measurement. A total of 5 μL of serum or 50 μL of FPLC fraction was used for cholesterol measurement. Triglycerides and cholesterol concentrations were determined according to the manufacturer's instructions using

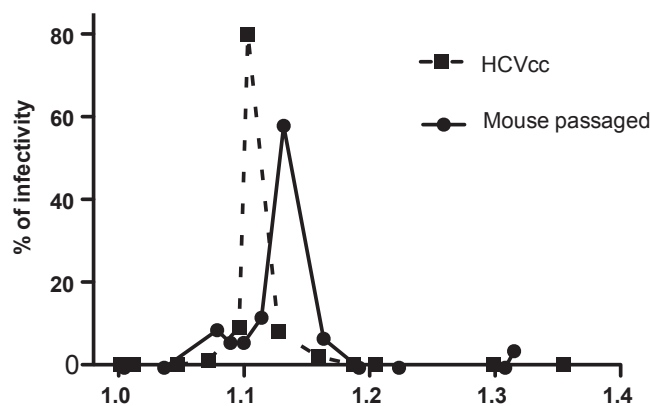


**Figure 1. Comparison of HCV infectivity buoyant density distribution between cell culture-derived and mouse-passaged J6/JFH1.** HCVcc prepared by electroporation of in vitro-transcribed viral RNA into Huh-7.5 cells and a mouse-passaged sample were used for buoyant density analysis. HCV particles were separated on 10%–40% iodixanol gradients. Twelve fractions were collected and HCV infectivity in each fraction was assessed by limiting dilution to determine TCID<sub>50</sub>/mL and are represented as the distribution of infectivity as a percentage of the total.

T-Cho and L-Type Triglycerides M from Wako Diagnostics (Richmond, VA).

### FPLC Analysis

Two Superose-6 FPLC columns in series were pre-equilibrated with buffer (0.15 mol/L NaCl, 1 mmol/L EDTA, pH 7.5). Samples were filtered through a membrane (pore size, 0.22 μm) to remove any particulate material, and 200 μL plasma was applied to the columns. Five mice plasma were pooled for each FPLC run. The flow rate was 0.4 mL/min, and 0.5-mL fractions were collected. Absorbance of the column effluent at a wavelength of 280 nm was monitored by a UV flow-through detector. The fractions corresponding to the lipoprotein particles noted earlier were determined by prior analysis of both mouse plasma and the human lipoproteins isolated by density gradient centrifugation (not shown).

### Iodixanol Isopicnic Gradient: 10%–40%

An equal volume of serum for each of the mice (range, 100–200 μL, depending on the time point) was diluted in phosphate-buffered saline (PBS) up to 1 mL and loaded in a 10%–40% continuous gradient iodixanol gradient achieved with Gradient Master (Biocomp, ND Canada). The gradient centrifugation was performed at 36,000 rpm for 16 hours using the SW41Ti rotor (Beckman Coulter, Brea, CA). The centrifugation was slowed with brake and stopped without brake and 12 fractions of 1 mL were collected.

### HCV-RNA Quantification

Total RNA was isolated from mouse serum using the QIAamp Viral RNA kit (Qiagen, Valencia, CA), and the HCV genome copy number was quantified by 1-step real-time polymerase chain reaction using a Multicode-RTx HCV RNA kit (Luminex Corp, Austin, TX) and a Roche LightCycler

480 (Roche Applied Science, Penzberg, Germany), according to the manufacturer's instructions.

### *Tissue Culture Infectious Dose 50 Assay*

Virus titration was performed by seeding Huh-7.5 cells in poly-L-lysine-coated 96-well plates at 6000 cells/well. Samples were serially diluted 10-fold in complete growth medium and used to infect the seeded cells (8 wells per dilution). After 3 days of incubation, the cells were immunostained for NS5A as described.<sup>29</sup> Briefly, cells were washed with PBS, fixed for at least 20 minutes with methanol (-20°C), and then washed. Washing consisted of 2 rinses with PBS and 1 rinse with PBS containing 0.1% (wt/vol) Tween. Cells were blocked for 30 minutes with PBS containing 0.1% (wt/vol) Tween, 1% (wt/vol) bovine serum albumin, and 0.2% (wt/vol) dried skim milk. Endogenous peroxidase activity was blocked further by a 5-minute incubation with PBS containing 0.3% (vol/vol) hydrogen peroxide, then washed. NS5A was detected by overnight incubation at 4°C with PBS containing 0.5% (wt/vol) Tween 100 and a 1:25,000 dilution of media from the 9E10 mouse monoclonal antibody.<sup>28</sup> After washing as described earlier, bound 9E10 was detected by a 1-hour incubation with anti-mouse polyclonal antibody conjugated with horseradish peroxidase and washed again, as described earlier. Bound peroxidase was detected with diaminobenzidine 7 tetrahydrochloride. Wells that contained at least 1 NS5A-expressing cell were counted as positive, and the TCID50 was calculated according to the method of Reed and Muench as referenced by Lindenbach.<sup>29</sup>

### *Western Blot*

A total of 10  $\mu$ L of each fraction was analyzed by Western blot using anti-apoE (52607-1:5000; Abcam, Cambridge, UK) and anti-apoC1 (198288-1:1000; Abcam). Proteins were separated on 4%–12% Bis-Tris NuPAGE polyacrylamide gels (Thermo Scientific) and transferred to 0.2- $\mu$ m nitrocellulose membranes. Membranes were blocked with 5% milk in Tris-buffered saline with 0.1% Tween 100 and probed with specific primary antibodies. After secondary antibody staining with peroxidase column purified donkey anti-rat IgG (H + L; 1:10,000), blots were visualized using SuperSignal West Dura reagent (ThermoFisher Scientific).

### *Statistical Analyses*

Statistical differences were analyzed using GraphPad Prism software (GraphPad Software, Inc, San Diego, CA). Data in which 2 groups were compared were analyzed using an unpaired *t* test. Data in which more than 2 groups were compared were analyzed by analysis of variance. *P* values less than .05 were considered significant.

## **Results**

### *Humanization of the Cholesterol Profile and Normalization of Triglycerides in Human Liver Chimeric FNRG Mice*

Differences between *in vitro*- and *in vivo*-derived HCV particles have been reported.<sup>22,23,30–32</sup> *In vivo*-derived

particles tend to be of lighter density and more infectious than *in vitro*-derived particles<sup>2,22</sup> and this may be because there is no human liver cell culture model that properly recapitulates VLDL biogenesis.<sup>8</sup> To test if the human liver chimeric FNRG mice could be used to address some of these differences we first set out to characterize the lipoprotein profile in this model. To do so, FNRG mice were transplanted with human hepatocytes and the degree of engraftment of these cells in the murine liver was monitored by quantification of human albumin in circulation as assessed by enzyme-linked immunosorbent assay.<sup>25</sup> Highly engrafted mice, defined as having human albumin levels greater than 1 mg/mL, were used to determine the lipoprotein profiles. As expected, and similar to what was reported by Ellis et al<sup>33</sup> in closely related human liver chimeric FRG mice, the cholesterol level was higher in mice after engraftment with human hepatocytes; furthermore, this cholesterol was carried mainly on VLDL and LDL as determined by FPLC, reflecting a typical human profile (Figure 2A and B). Surprisingly, we found that the triglyceride levels in FNRG mice before transplantation were increased slightly compared with normal values in C57-BL6 wild-type mice (<100 mg/dL) or in non-obese diabetic-SCID (57.4 mg/dL) (Figure 2C). VLDL triglyceride levels decreased significantly upon humanization and redistributed between VLDL and intermediate-density lipoprotein/LDL (Figure 2D). The high level of triglycerides in the FNRG mice compared with reported values in other mice could result from the *fah* deficiency or could be owing to the difference in genetic background. Thus, to dissect this phenotype further, we measured triglyceride levels from untransplanted FNRG, NRG, and FRG mice. The total triglyceride levels from the FRG mice were increased to greater than those determined for NRG mice, although they did not reach FNRG levels (Figure 3A). When analyzed by FPLC (Figure 3B and C), the triglyceride levels in the VLDL fraction was comparable between FRG and FNRG mice. These results indicate that the *fah* deficiency affects baseline triglyceride levels. Taken together, human liver chimeric FNRG mice show a human-like lipoprotein profile and reconstitution of the *fah* by the human liver xenograft is sufficient to restore triglycerides to normal levels. These findings support the use of the human liver chimeric FNRG mice as a suitable model for human lipoprotein metabolism studies as well as HCV/lipoprotein association studies.

### *HCV Buoyant Density in FNRG Mice Evolves Over Time*

Thirteen highly engrafted human liver chimeric FNRG mice were challenged with J6/JFH1 that had been passaged in humanized FNRG mice and the biophysical properties of the virus were monitored. After 2 weeks of infection, sera were collected and virus particles were separated based on their densities. All of the mice had detectable HCV-RNA levels and the amount of infectious particles (TCID50/mL) was similar to the 4 mice selected for representation in Figure 4 (left panel). For 8 of 10 mice, 2 major peaks of viral RNA were detected and were associated with the presence of infectious particles. A third RNA peak of even higher density



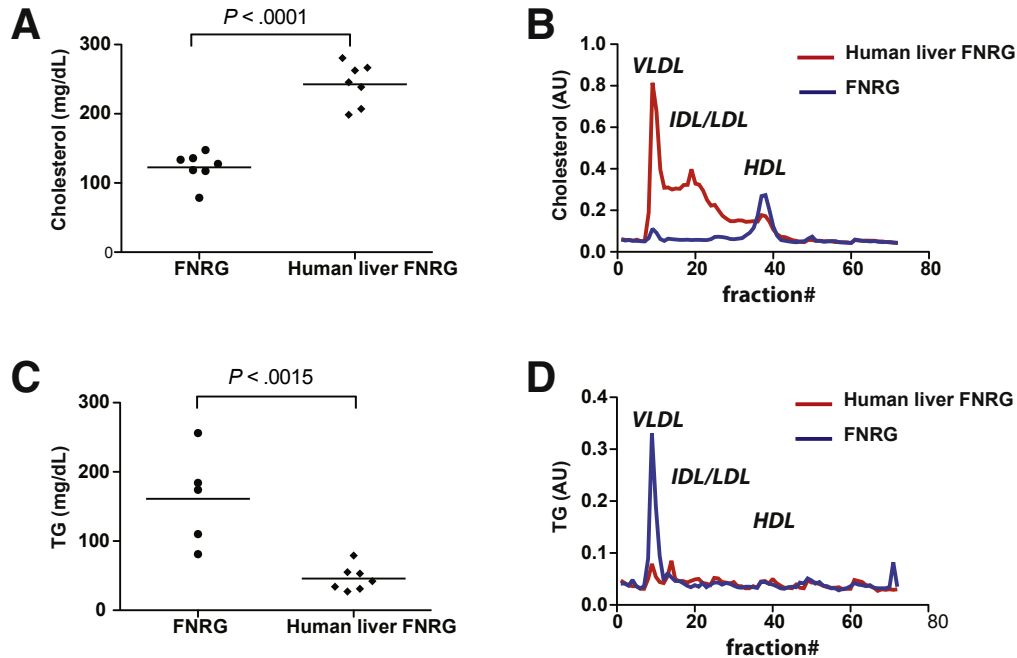


**Figure 2. Lipoprotein profiles of FNRG and human liver chimeric FNRG mice.** (A) Total cholesterol and (C) triglyceride (TG) levels were measured in the serum of FNRG and noninfected human liver chimeric FNRG mice that were highly engrafted (defined as having  $> 1$  mg/mL human serum albumin levels) using commercial diagnostic kits (WAKO). Statistical differences were analyzed using an unpaired  $t$  test ( $n = 7$ ). (B and D) Lipoprotein profiles of FNRG and noninfected human liver chimeric FNRG mice were determined by FPLC using pooled plasma ( $n = 5$ ). The fractions corresponding to the lipoprotein particles noted in the figure were determined by prior analysis of lipoproteins derived from both mouse and human plasma by density gradient centrifugation. (B) Cholesterol and (D) triglyceride content in each fraction was determined using commercial diagnostic kits (WAKO). AU, arbitrary unit.

( $>1.3$  g/mL), but associated with reduced infectivity, was present for one of the serum samples analyzed (7343). The amount of infectivity associated with the low-density peak ( $<1.1$  g/mL) was higher than that associated with the high-density peak ( $\approx 1.15$ – $1.19$  g/mL). Indeed, specific infectivity of the low-density fraction was close to 1 TCID<sub>50</sub> per RNA molecule (Figure 4C), whereas at higher density, specific infectivity was 1 TCID<sub>50</sub> for 100–1000 RNA molecules. To further investigate the variation of HCV particle buoyant density over time, we performed the same analysis on serum collected at 5 weeks after infection (Figure 4A, right panel). At this later time point, we observed a significant decrease of specific infectivity in the low-density fractions (Figure 4B and C). Together, these data show that the buoyant density distribution of HCV early after infection was as expected, with low density and high specific infectivity. Interestingly, the third peak (density  $> 1.3$  g/mL) appeared in 2 additional sera compared with the first time point (7343, 7337, 7339). To summarize, at 5 weeks after infection a redistribution of the specific infectivity was observed, with a reduced proportion of lighter and more infectious particles.

The heterogeneity of in vivo- and in vitro-derived particles<sup>12,13,32,34–36</sup> has been described extensively, and is thought to be owing to differences in the biochemical nature of the particles. In our data, the lightest peak of infectivity observed could correspond to the nucleocapsid-free LVPs.<sup>34</sup> Unfortunately, the quantity of material available in this

study was not sufficient to directly assess the composition of virions at particular densities or detect viral proteins in the fractions. Nonetheless, as shown in Figure 4D, we compared the 2-week and 5-week gradient for the co-distribution of apolipoprotein (apoE and apoC1). ApoC1 was found to be the lightest fraction, whereas apoE was found mainly in the 5 lightest fractions with detectable amounts also observed in the adjacent 3 consecutive fractions. ApoE<sup>15–18</sup> and apoC1<sup>37,38</sup> have been reported as essential factors of HCV infectivity. We did not observe redistribution of these 2 proteins between the 2 time points. Further characterization of the particles using immunoelectron microscopy or mass spectrometry could help determine the different nature of the particles and show key components of their infectivity.

#### *HCV Buoyant Density Distribution Is Impacted Minimally by Sucrose Feeding During the Fed State*

As reported by Felmler et al.,<sup>39</sup> dietary lipids have been shown to influence the release of HCV in the circulation in human beings by increasing the amount of detectable HCV RNA in the VLDL fraction after ingestion of a high-fat meal (milkshake). As a reference, we compared the mouse-passaged virus used for infection of the mice with cell cultured-derived virus (Figure 1). To assess how diet-induced

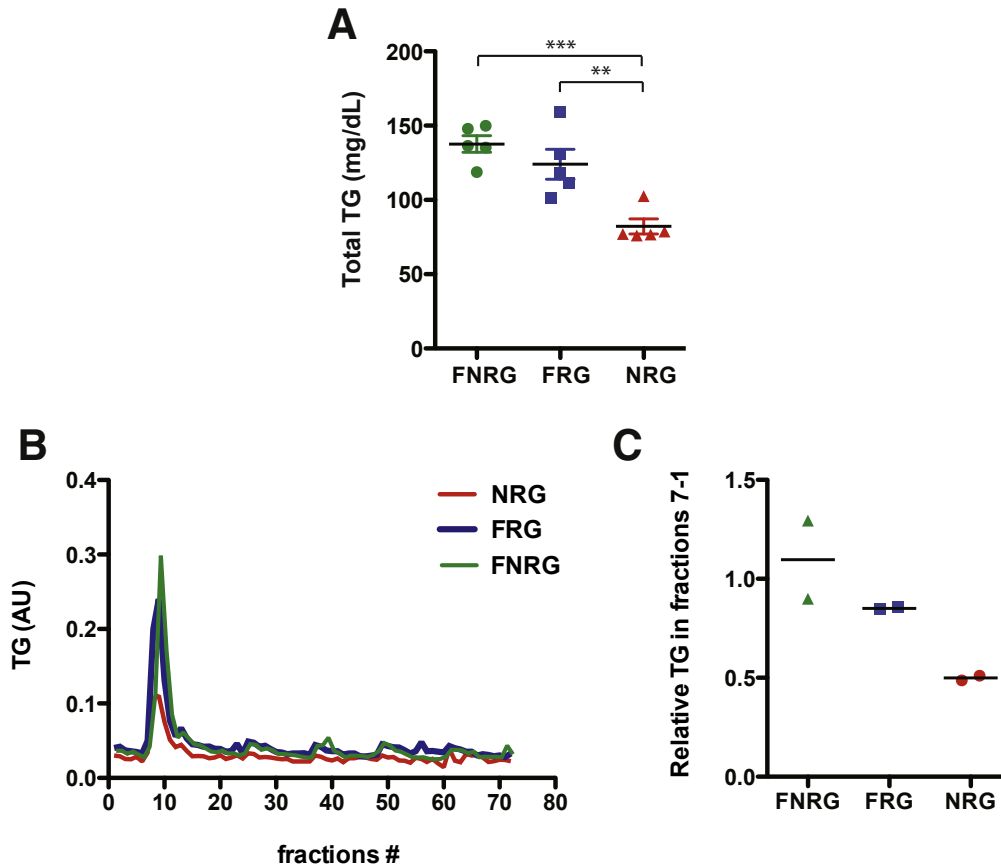
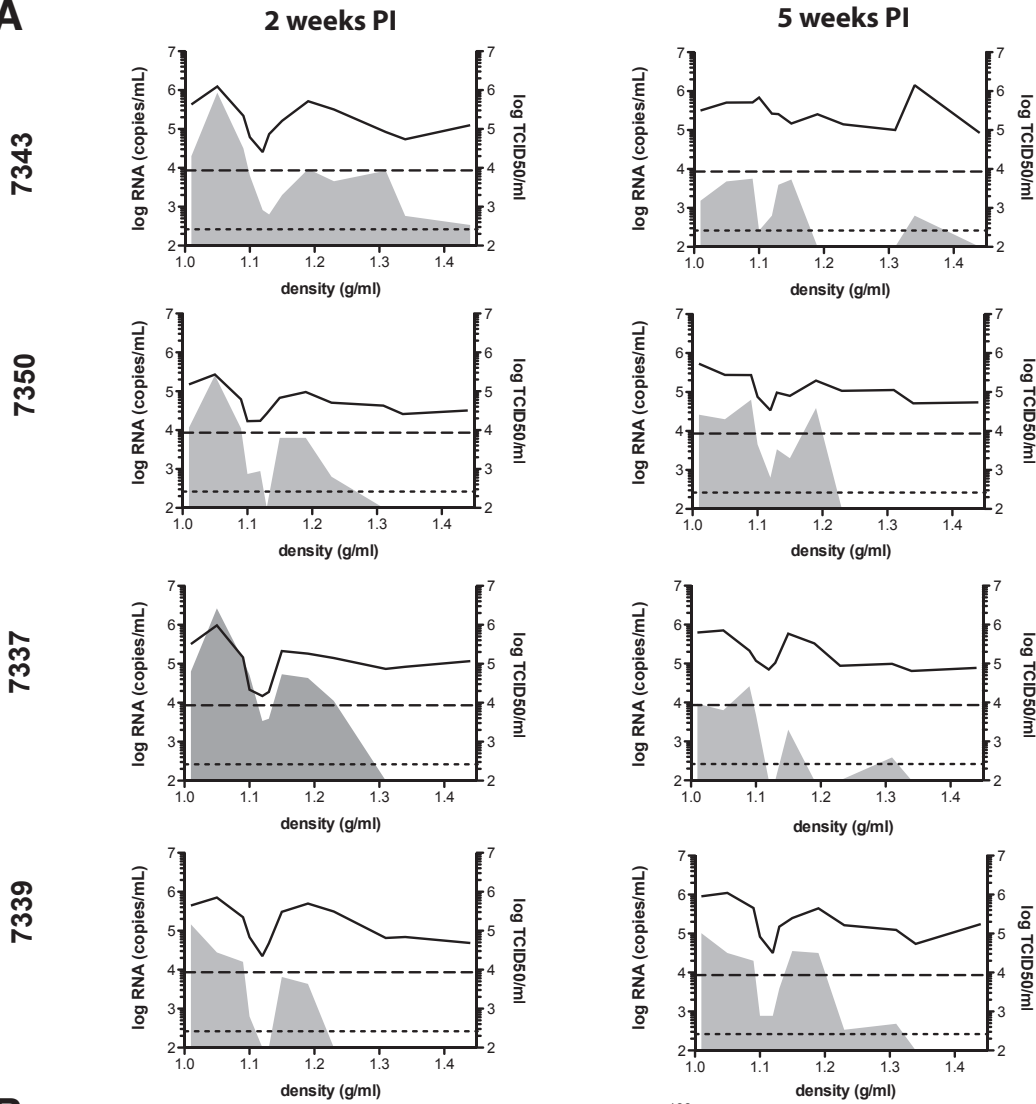


**Figure 3. Triglyceride (TG) profiles of FNRG, NRG, and FRG mice.** (A) Total triglyceride levels were measured in the serum of FNRG, NRG, and FRG using commercial diagnostic kits (WAKO). Statistical differences were compared by analysis of variance using the Bonferroni multiple comparison test (\*\* $P < .01$ ; \*\*\* $P < .001$ ) ( $n = 5$ ). (B and C) Lipoprotein profiles of FNRG, NRG, and FRG mice were determined by FPLC. The fractions corresponding to the lipoprotein particles noted in the figure were determined by prior analysis of lipoproteins derived from both mouse and human plasma by density gradient centrifugation. The tracing comes from the mean of 2 experiments of pooled plasma ( $n = 5$ ). (C) Triglyceride content in each fraction was determined using commercial diagnostic kits (WAKO). (C) The relative content of triglycerides in the peak fractions is represented for each of the 2 experiments. AU, arbitrary unit.

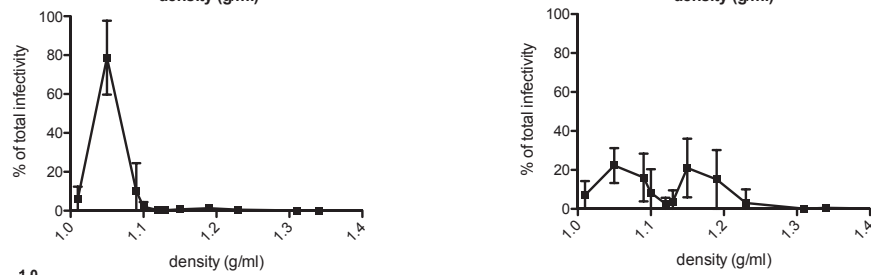
manipulation of host metabolism might affect HCV heterogeneity and infectivity, a group of 5 mice were given 10% sucrose in their drinking water (Figure 5A). This has been described to promote VLDL lipidation and secretion in rodents.<sup>40</sup> As expected, we observed a significant increase in triglyceride levels as well as cholesterol content in VLDL and LDL by FPLC in noninfected mice after 5 weeks of sucrose feeding (Figure 6A and B). In mice infected with HCV and then placed on a sucrose diet for 2 weeks, no significant differences in HCV buoyant density were observed compared with infected mice on a regular diet (control) (Figure 5C), and both groups (sucrose and control) lost infectivity in the lower-density fractions compared with the earlier time point (Figure 5B vs C). After 5 weeks on sucrose, we observed a slight shift of the higher density peak from 1.15 g/mL (fraction 7) to 1.1 g/mL (fraction 5) (Figure 5D). To establish if this was attributable to changes in the biogenesis of the LVP, we analyzed the distribution of infectivity after overnight fasting because this would reduce the chylomicron contribution to the VLDL fraction. Interestingly, the

distribution profile after overnight fasting (at 8 wk) (Figure 5E) became comparable with the distribution observed early after infection (at 2 wk), at which the majority of infectivity was detected in a single peak at low density (Figure 5B). Notably, we did not observe any differences with or without sucrose under these conditions. Sucrose was withdrawn after harvesting at the 11-week postinfection time point (8 weeks  $\pm$  sucrose) and we continued to analyze the evolution of the HCV buoyant density distribution of the virus from the 2 groups of mice after sucrose withdrawal (Figure 5F and G). The overall infectivity decreased further for the mice still alive (Table 1), and the distribution of the denser peak shifted slightly toward lower density with no differences between the 2 groups at 3 weeks or 6 weeks after sucrose withdrawal. Overall, these data indicate that the effect of a 10% sucrose diet on HCV buoyant density was minimal in FNRG mice and was observed only after feeding when the mice had been on sucrose for 5 weeks. Furthermore, the effect was transient because it did not persist after sucrose withdrawal.

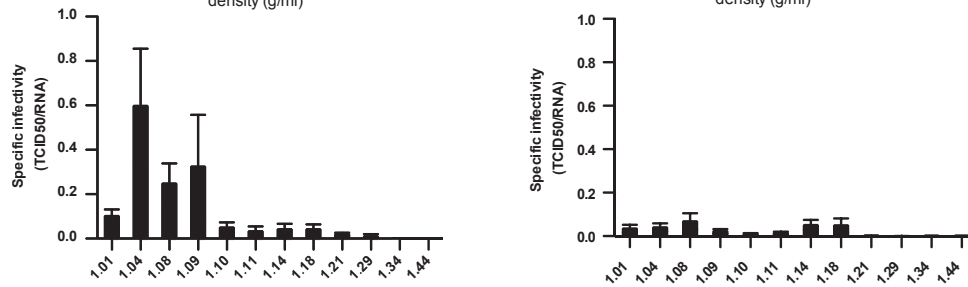
**A**



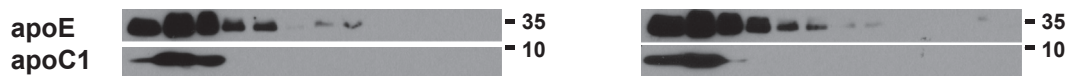
**B**



**C**



**D**



### Effect of Sucrose Feeding on Lipoprotein Metabolism

To determine if the modest difference noted at 8 weeks after infection between the 2 groups with or without sucrose (5 weeks  $\pm$  sucrose) could be attributed to any change in lipoprotein composition, we analyzed the cholesterol and triglyceride content of each fraction (Figure 6A and B). We observed that fraction 5, which contained increased infectivity after 5 weeks of sucrose compared with control mice, also contained higher levels of triglycerides and cholesterol (Figure 6C and D). Thus, the impact of the sucrose diet on HCV particle density correlates with the appearance of a fraction containing higher triglyceride and cholesterol levels compared with control mice.

Taking all of our results together, we show how distribution of the infectivity of HCV particles evolves in vivo. In human liver, chimeric FNRG mice HCV circulates as a population of particles of light as well as dense buoyant densities and both are infectious. Changes in diet as well as conditions such as fasting and feeding affect the distribution of HCV buoyant density gradients.

### Discussion

Heterogeneity of virus particles is a particular feature of HCV in part because of its ability to associate with lipoproteins. Although the development of a cell culture system to study HCV in vitro has enabled the discovery of essential host factors for HCV assembly, such as apoE,<sup>15–18</sup> none of the cell lines that are used to produce HCV particles fully recapitulate VLDL assembly.<sup>21</sup> It remains unclear if HCV assembly and particle composition truly mimic HCV as a lipovirion particle in human circulation. Articles presenting experiments in which HCVcc was passaged from cell culture to animal models (chimpanzees or liver chimeric Alb-uPA mice) or liver chimeric FRG mice<sup>22,30</sup> only reported representative buoyant density profiles that originated from a single time point or from pooled samples harvested at different time points. In this study, we showed that HCV buoyant density and infectivity change over time and are influenced by dietary changes.

We show that the humanized FNRG mouse model is suitable for human lipoprotein metabolism studies. The cholesterol profile of the human hepatocyte-engrafted FNRG mice appeared humanized with a redistribution of the cholesterol from HDL to LDL and VLDL consistent with data from the human liver chimeric FRG mouse model.<sup>33</sup> We

observed somewhat increased plasma triglyceride levels in the nontransplanted FNRG mice, likely owing to the fah deficiency. The human hepatocytes express FAH and we observed a reduction of the triglyceride levels upon efficient engraftment and expansion of these cells in the murine liver. These results support the use of the human FNRG liver chimeric mouse model as an animal model to study lipoprotein metabolism. Notably, in human beings, the cholesterol ester transfer protein (CETP) transfers cholesterol in the circulation from HDL to VLDL.<sup>8</sup> However, intravascular lipoprotein metabolism differs in mice because they lack expression of CETP,<sup>8</sup> and thus carry most of their cholesterol on HDL, as opposed to human beings who carry cholesterol mainly on VLDL and LDL. High LDL is a risk factor for developing coronary artery disease and our results show that humanized FNRG mice provide a promising model for studies of human lipoprotein metabolism in vivo. CETP inhibitors held great promise until the recent termination of the A Study of Evacetrapib in High-Risk Vascular Disease (Eli Lilly and company) phase II study<sup>41</sup> in which the CETP inhibitor evacetrapib showed efficiency at reducing LDL cholesterol and increasing HDL that, however, failed in translating into a clinical outcome of reduced cardiovascular events.<sup>42</sup> These results underscore the need for a better mechanistic understanding of the dynamic of lipoprotein metabolism and its contribution to cardiovascular events. Humanized mouse models could constitute a valuable tool for such studies.

Having established that the human liver chimeric FNRG model showed humanized lipoprotein profiles, we next investigated the biophysical properties of the HCV particles generated in these mice. HCV particles present in the serum of HCV-infected patients are mainly of low density (1.006–1.15 g/mL) owing to association of the particles with lipoproteins. Our results looking at HCV particle density early after infection were similar to what was reported by Lindenbach et al<sup>22</sup> and Maillard et al<sup>32</sup> using the same virus (J6/JFH1) in the SCID/Alb-uPA human liver chimeric mouse model. These results are consistent with data obtained in chimpanzees in which infectivity was correlated inversely with their buoyant density.<sup>11,22</sup> HCV association with lipoproteins is thought to occur intracellularly; however, Felmler et al<sup>39</sup> reported that HCV RNA can be recovered from the triglyceride-rich lipoprotein fraction after a high-fat meal and reported that HCV was able to transfer to triglyceride-rich lipoproteins in vitro. These results suggested that HCV could associate with lipoproteins extracellularly, especially chylomicrons. However,

**Figure 4.** (See previous page). **Buoyant density distribution of HCV RNA and infectivity at 2 and 5 weeks after infection.** (A) Sera of 4 representative liver chimeric mice (numbered 7343, 7350, 7337, 7339) infected with J6/JFH1 were collected. HCV particles were separated on a 10%–40% iodixanol gradient. Twelve fractions of 1 mL were collected. HCV RNA was quantified by quantitative reverse-transcription polymerase chain reaction in each fraction (represented by the *black line graph*), and HCV infectivity in each fraction was assessed by limiting dilution to determine TCID<sub>50</sub>/mL (represented by the *filled gray area*). Each mouse number is indicated. (B) The percentage of total infectivity (TCID<sub>50</sub> in each fraction/sum of TCID<sub>50</sub> in all fractions) in each fraction of corresponding density is represented for 2 weeks after infection (*left*) and for 5 weeks after infection (*right*). (C) Specific infectivity was calculated for each fraction by dividing the number of infectious particles (TCID<sub>50</sub>/mL) with the number of RNA molecules (HCV RNA copies/mL). The more infectious the virus is the closest to one the specific infectivity. (D) Analysis of the immunoreactivity of the fractions to apoE and apoC1 by Western blot for 2 weeks after infection (*left*) and 5 weeks after infection (*right*). Representative immunoblots are shown.



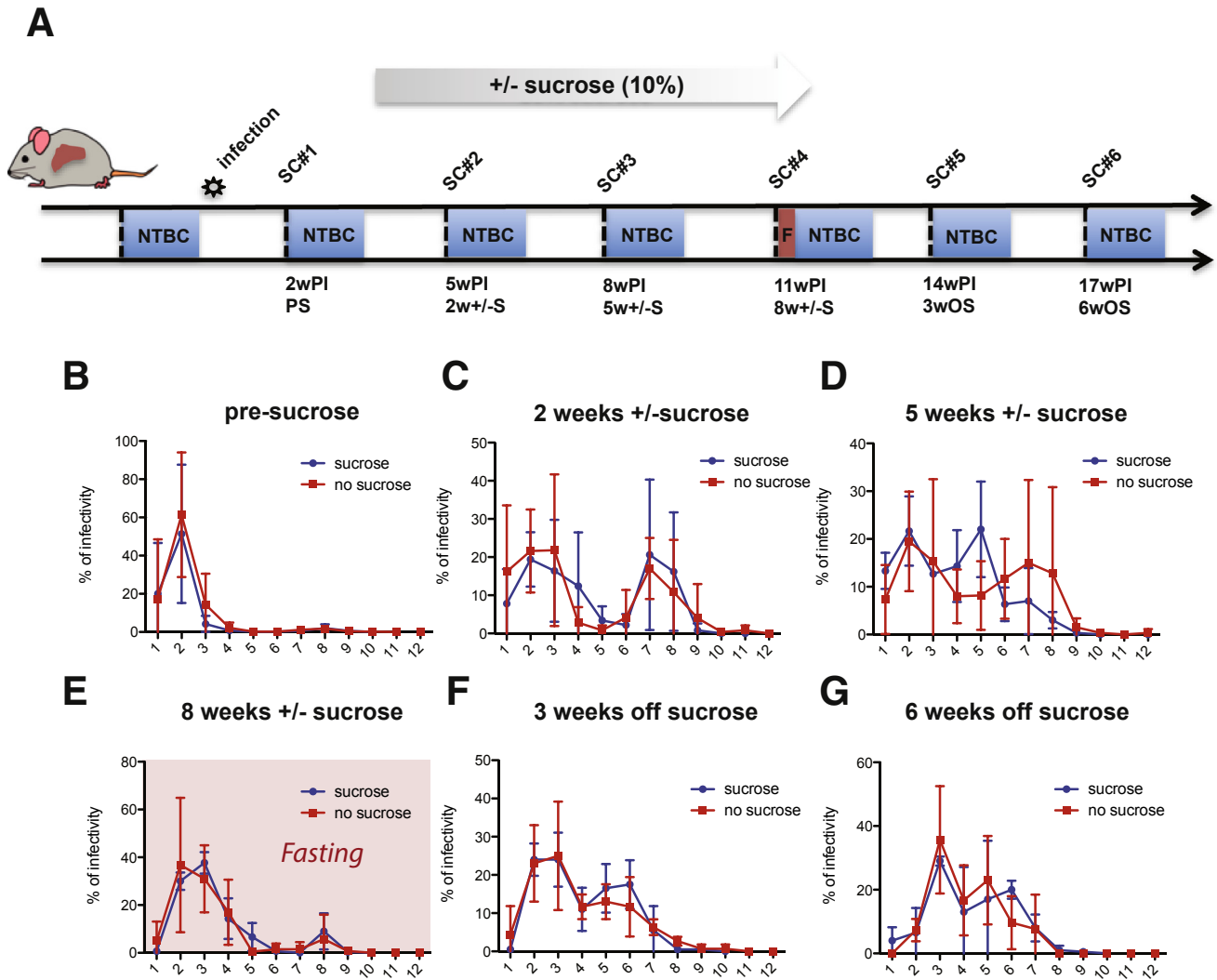


**Figure 5. Effect of 10% sucrose feeding on HCV infectivity buoyant density distribution.** (A) Schematic of the experiment outline. A group of 13 human liver chimeric FNRG mice were infected with J6/JFH1 and serum was collected every 3 days before NTBC cycling to perform gradient density fractionation. After 2 weeks, 5 mice were given 10% sucrose in their drinking water for 8 weeks and then sucrose was withdrawn and the experiment was continued for 2 more weeks before killing the animals. At 11 weeks after infection, the mice were fasted overnight before serum collection. PS, presucrose; SC, serum collection; w ± S, weeks ± sucrose; wOS, weeks off sucrose; wPI, weeks postinfection. (A–C) Difference in buoyant density distribution of HCV infectivity between sucrose-fed mice and control mice (no sucrose). Thirteen mice were separated into 2 groups: one group (5 mice) received 10% sucrose in the drinking water at 2 weeks after infection (blue), and the other group received water as a control (red). The blood of infected human liver chimeric FNRG mice was collected at (B) 2, (C) 5, (D) 8, (E) 11, (F) 14, and (G) 17 wPI. Before the 11 wPI blood draw, mice were fasted overnight. HCV particles were separated on a 10%–40% iodixanol gradient. Twelve fractions were collected and HCV infectivity in each fraction was assessed by limiting dilution to determine TCID<sub>50</sub>/mL. The distribution of infectivity is represented as a percentage of the total as indicated in Figure 4B.

the ability of this transfer to alter infectivity could not be addressed in their study.

As reported in other in vivo models,<sup>22,30,32</sup> we showed that HCV is heterogeneous in the sera of the humanized FNRG mice with a higher proportion of particles of low density and high infectivity early after infection. However, we observed a redistribution of the virus over the course of the infection, with more particles of higher density and a decrease of specific infectivity. Because other studies only

looked at single time points or pooled samples over time, the dynamics of HCV particles over time has been largely overlooked.<sup>22,32</sup> In human beings, the presence of immune complexes of antibodies with viral particles has been suggested to alter the density of the particles toward higher densities.<sup>11</sup> Because FNRG animals are severely immunocompromised and cannot make HCV antibodies, the appearance of a population of higher density cannot result from the formation of immune complexes. Rather, the

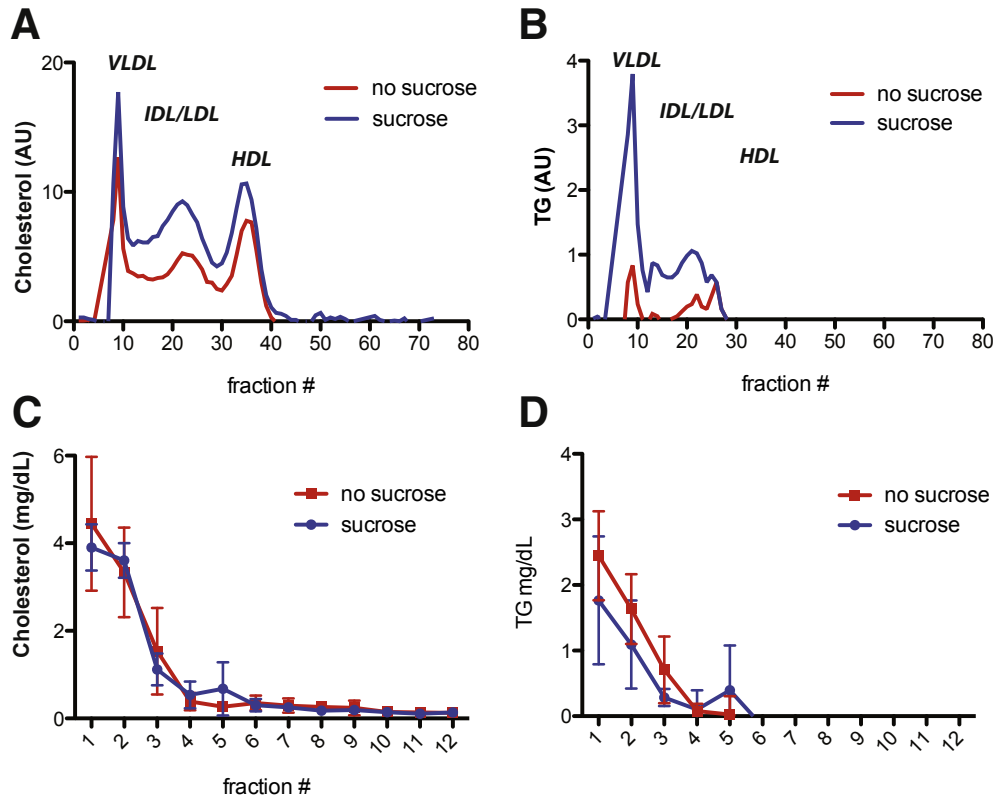


**Figure 6. Cholesterol and triglyceride content of fractionated mouse serum after 5 weeks of 10% sucrose feeding compared with control.** (A and B) Lipoprotein profiles of noninfected human liver chimeric FNRG mice fed 10% sucrose or not in their drinking water were determined by FPLC. The fractions corresponding to the lipoprotein particles noted in the figure were determined by prior analysis of lipoproteins derived from both mouse and human plasma by density gradient centrifugation. (A) Cholesterol and (B) triglyceride (TG) content in each fraction was determined using commercial diagnostic kits (WAKO). (C and D) A total of 50 uL and 100 uL from each fraction of iodixanol were used to measure (C) cholesterol and (D) triglyceride levels, respectively, using a commercial diagnostic kit (Wako). AU, arbitrary unit; IDL, intermediate-density lipoprotein.

denser particles are either formed in the liver or are the result of the remodeling of lipoprotein components of the LVP by serum enzymes such as lipoprotein lipase and

CETP. The highest density peak could represent a fraction of the virus less enriched in lipoprotein or of nonenveloped nucleocapsids.<sup>43</sup> Interestingly, recent work by Piver et al<sup>44</sup>

**Table 1. Average Infectivity (TCID50/mL) per Fraction for Each Time Point**

Average infectivity (TCID50/mL)	Bleed 1	Bleed 2	Bleed 3	Bleed 4	Bleed 5	Bleed 6
1	4.6E+04	1.6E+04	9.8E+03	2.7E+02	7.2E+02	9.2E+02
2	5.6E+05 <sup>a</sup>	1.6E+04	3.9E+04	3.2E+03	7.5E+03 <sup>a</sup>	9.5E+02
3	1.9E+05	1.7E+04 <sup>a</sup>	2.4E+04	3.6E+03 <sup>a</sup>	7.4E+03	5.0E+03 <sup>a</sup>
4	3.6E+04	2.6E+03	1.1E+04	1.9E+03	2.6E+03	1.9E+03
5	3.7E+03	5.1E+02	1.3E+04	5.3E+02	3.7E+03	3.6E+03
6	5.1E+03	1.4E+03	1.7E+04	1.6E+02	5.0E+03	2.5E+03
7	9.9E+03	9.6E+03	2.9E+04	6.2E+01	8.1E+02	1.9E+03
8	1.5E+04	9.3E+03	4.4E+04 <sup>a</sup>	5.1E+02	3.2E+02	6.3E+02
9	6.1E+03	2.1E+02	1.2E+03	1.4E+02	1.8E+02	4.3E+02
10	1.4E+03	9.6E+01	1.3E+03	1.0E+00	9.4E+01	ND
11	1.1E+02	7.1E+01	3.8E+01	1.0E+00	ND	ND
12	6.5E+01	1.0E+01	1.1E+03	1.0E+00	ND	ND

NOTE. TCID50/mL have been averaged for each fraction number. ND, not determined.  
<sup>a</sup>Fraction with the highest density per time point.

compared the ultrastructure of serum and HCVcc particles (LVP) and reported that they are comparable in their composition and association with lipoproteins. Therefore, one can speculate that the true nature of the particles is comparable between *in vitro*- and *in vivo*-derived material, but that the stoichiometry between apolipoprotein components and lipids is altered, thus affecting the infectivity. Notably, the *in vitro*-derived material does not represent particles that have been subjected to intravascular remodeling *in vivo*. We recently reported that expression of Sec14L2 allowed the replication of clinical isolates in Huh-7.5 *in vitro*.<sup>45</sup> Taking advantage of this system, future work may be able to analyze the infectivity of HCV particles derived from HCV-infected individuals after passaging *in vitro* if high levels of highly infectious patient material are available in sufficient quantity to see a signal after fractionation on gradients.

Regarding decreased overall infectivity, we know from previous experiments that human albumin levels in mice highly engrafted with human hepatocytes reach greater than 1 mg/mL and are maintained over several NTBC cycles, indicating a persistence of the graft. In this particular study, human albumin levels measured at the end point of the experiment for surviving mice was all greater than the 1 mg/mL level (data not shown). Thus, it is unlikely that the decrease of infectivity of the virus over time was owing to loss of the human graft. Alternatively, the decreased infectivity over time could be owing to the bottleneck imposed by the infection on the quasispecies diversity.

In an attempt to manipulate lipoprotein biogenesis *in vivo*, we put the mice on a diet known to promote VLDL formation in rats and investigated the effect on the biophysical properties of the virus. The impact on HCV infectivity and buoyant density of the sucrose diet was minimal, yielding only a slight shift toward lower buoyant density. Nevertheless, this shift correlated with a trend toward enhanced triglyceride and cholesterol levels in the same fractions. To better explore whether perturbing the VLDL secretion pathway could affect the biophysical properties of the virus, another diet, such as a high-fat diet, might be considered in future studies. A high-fat diet might have a more significant impact on the lipoprotein profile in this humanized mouse model. In the present study, we also tested the effect of fasting and, interestingly, we observed that fasting gave rise to a shift toward more low-density particles, similar to what we had seen early after infection. A direct comparison of fasting vs feeding is needed to confirm this result. However, at 2 weeks after infection, fasting was the only condition that minimized the presence of infectious particles at higher densities, and we speculate that in a fasting state, when insulin is low, VLDL secretion is not inhibited<sup>46</sup> and circulating chylomicrons<sup>8</sup> are low, circulating HCV reflects what emerges from the liver cells: either a VLDL-HCV chimeric particle or a HCV particle quickly transferred to VLDL after secretion by the hepatocyte. The more heterogeneous profile seen during the fed state compared with the fasted state suggests a role of the transfer of HCV among lipoprotein classes orchestrated by

serum enzymes such as CETP and Lipoprotein Lipase in the circulation. We think it is unlikely to be an effect of virus selection because a single overnight fast at 11 weeks after infection is sufficient to restore a majority of the infectivity in the low-density fractions and in a reversible manner. The impact of metabolic changes on virus pathogenesis has been poorly studied. A recent article<sup>47</sup> showed how glucose utilization needed to be preserved to resist viral infection in mice, linking the phenotype to innate immune response. Therefore, the effect of fasting might be affecting the viral pathogenesis at several levels related not only to lipoprotein metabolism.

We did not address interindividual variability in our study because only 1 human hepatocyte donor was used to generate the human liver chimeric mice. Nevertheless, one could use this model to seek insights into how the host cells impact the physical properties of the virus, generating human liver chimeric mice from different human hepatocyte sources, as recently was shown with LDL-receptor-deficient hepatocytes.<sup>48</sup>

## Conclusions

In summary, our data present the evolution of HCV infectivity over time and the biophysical properties of the HCV particles in the human liver chimeric FNRG mouse model. HCV circulates as low and high buoyant density particles *in vivo* and the respective distribution between lipoprotein classes depends on dietary changes including fed and fasting states.

## References

1. Yamane D, McGivern DR, Masaki T, Lemon SM. Liver injury and disease pathogenesis in chronic hepatitis C. *Curr Top Microbiol Immunol* 2013;369:263–288.
2. Adinolfi LE, Restivo L, Zampino R, Guerrera B, Lonardo A, Ruggiero L, Riello F, Loria P, Florio A. Chronic HCV infection is a risk of atherosclerosis. Role of HCV and HCV-related steatosis. *Atherosclerosis* 2012; 221:496–502.
3. Roed T, Lebech AM, Kjaer A, Weis N. Hepatitis C virus infection and risk of coronary artery disease: a systematic review of the literature. *Clin Physiol Funct Imaging* 2012;32:421–430.
4. Paul D, Madan V, Bartenschlager R. Hepatitis C virus RNA replication and assembly: living on the fat of the land. *Cell Host Microbe* 2014;16:569–579.
5. Popescu CI, Riva L, Vlaicu O, Farhat R, Rouille Y, Dubuisson J. Hepatitis C virus life cycle and lipid metabolism. *Biology (Basel)* 2014;3:892–921.
6. Lindenbach BD, Rice CM. The ins and outs of hepatitis C virus entry and assembly. *Nat Rev Microbiol* 2013; 11:688–700.
7. Bassendine MF, Sheridan DA, Bridge SH, Felmlee DJ, Neely RD. Lipids and HCV. *Semin Immunopathol* 2013; 35:87–100.
8. Cohen DE, Fisher EA. Lipoprotein metabolism, dyslipidemia, and nonalcoholic fatty liver disease. *Semin Liver Dis* 2013;33:380–388.

9. Ginsberg HN, Fisher EA. The ever-expanding role of degradation in the regulation of apolipoprotein B metabolism. *J Lipid Res* 2009;50(Suppl):S162–S166.
10. Prince AM, Huima-Byron T, Parker TS, Levine DM. Visualization of hepatitis C virions and putative defective interfering particles isolated from low-density lipoproteins. *J Viral Hepat* 1996;3:11–17.
11. Bradley D, McCaustland K, Krawczynski K, Spelbring J, Humphrey C, Cook EH. Hepatitis C virus: buoyant density of the factor VIII-derived isolate in sucrose. *J Med Virol* 1991;34:206–208.
12. Catanese MT, Uryu K, Kopp M, Edwards TJ, Andrus L, Rice WJ, Silvestry M, Kuhn RJ, Rice CM. Ultrastructural analysis of hepatitis C virus particles. *Proc Natl Acad Sci U S A* 2013;110:9505–9510.
13. Merz A, Long G, Hiet MS, Brugger B, Chlanda P, Andre P, Wieland F, Krijnse-Locker J, Bartenschlager R. Biochemical and morphological properties of hepatitis C virus particles and determination of their lipidome. *J Biol Chem* 2011;286:3018–3032.
14. Fauvelle C, Felmlee DJ, Crouchet E, Lee J, Heydmann L, Lefevre M, Magri A, Hiet MS, Fofana I, Habersetzer F, Fong SK, Milne R, Patel AH, Vercauteren K, Meuleman P, Zeisel MB, Bartenschlager R, Schuster C, Baumert TF. Apolipoprotein E mediates evasion from hepatitis C virus neutralizing antibodies. *Gastroenterology* 2016;150:206–217.
15. Chang KS, Jiang J, Cai Z, Luo G. Human apolipoprotein E is required for infectivity and production of hepatitis C virus in cell culture. *J Virol* 2007;81:13783–13793.
16. Huang H, Sun F, Owen DM, Li W, Chen Y, Gale M Jr, Ye J. Hepatitis C virus production by human hepatocytes dependent on assembly and secretion of very low-density lipoproteins. *Proc Natl Acad Sci U S A* 2007;104:5848–5853.
17. Jiang J, Luo G. Apolipoprotein E but not B is required for the formation of infectious hepatitis C virus particles. *J Virol* 2009;83:12680–12691.
18. Da Costa D, Turek M, Felmlee DJ, Girardi E, Pfeffer S, Long G, Bartenschlager R, Zeisel MB, Baumert TF. Reconstitution of the entire hepatitis C virus life cycle in nonhepatic cells. *J Virol* 2012;86:11919–11925.
19. Fukuhara T, Wada M, Nakamura S, Ono C, Shiokawa M, Yamamoto S, Motomura T, Okamoto T, Okuzaki D, Yamamoto M, Saito I, Wakita T, Koike K, Matsuura Y. Amphipathic alpha-helices in apolipoproteins are crucial for the formation of infectious hepatitis C virus particles. *PLoS Pathog* 2014;10:e1004534.
20. Herker E, Harris C, Hernandez C, Carpentier A, Kaehlicke K, Rosenberg AR, Farese RV Jr, Ott M. Efficient hepatitis C virus particle formation requires diacylglycerol acyltransferase-1. *Nat Med* 2010;16:1295–1298.
21. Meex SJ, Andreo U, Sparks JD, Fisher EA. Huh-7 or HepG2 cells: which is the better model for studying human apolipoprotein-B100 assembly and secretion? *J Lipid Res* 2011;52:152–158.
22. Lindenbach BD, Meuleman P, Ploss A, Vanwolleghem T, Syder AJ, McKeating JA, Lanford RE, Feinstone SM, Major ME, Leroux-Roels G, Rice CM. Cell culture-grown hepatitis C virus is infectious in vivo and can be recultured in vitro. *Proc Natl Acad Sci U S A* 2006;103:3805–3809.
23. Steenbergen RH, Joyce MA, Lund G, Lewis J, Chen R, Barsby N, Douglas D, Zhu LF, Tyrrell DL, Kneteman NM. Lipoprotein profiles in SCID/uPA mice transplanted with human hepatocytes become human-like and correlate with HCV infection success. *Am J Physiol Gastrointest Liver Physiol* 2010;299:G844–G854.
24. Grompe M, Lindstedt S, al-Dhalimy M, Kennaway NG, Papaconstantinou J, Torres-Ramos CA, Ou CN, Finegold M. Pharmacological correction of neonatal lethal hepatic dysfunction in a murine model of hereditary tyrosinaemia type I. *Nat Genet* 1995;10:453–460.
25. de Jong YP, Dorner M, Mommersteeg MC, Xiao JW, Balazs AB, Robbins JB, Winer BY, Gerges S, Vega K, Labitt RN, Donovan BM, Giang E, Krishnan A, Chiriboga L, Charlton MR, Burton DR, Baltimore D, Law M, Rice CM, Ploss A. Broadly neutralizing antibodies abrogate established hepatitis C virus infection. *Sci Transl Med* 2014;6:254ra129.
26. Blight KJ, McKeating JA, Rice CM. Highly permissive cell lines for subgenomic and genomic hepatitis C virus RNA replication. *J Virol* 2002;76:13001–13014.
27. Grompe M, al-Dhalimy M, Finegold M, Ou CN, Burlingame T, Kennaway NG, Soriano P. Loss of fumarylacetoacetate hydrolase is responsible for the neonatal hepatic dysfunction phenotype of lethal albino mice. *Genes Dev* 1993;7:2298–2307.
28. Lindenbach BD, Evans MJ, Syder AJ, Wolk B, Tellinghuisen TL, Liu CC, Maruyama T, Hynes RO, Burton DR, McKeating JA, Rice CM. Complete replication of hepatitis C virus in cell culture. *Science* 2005;309:623–626.
29. Lindenbach BD. Measuring HCV infectivity produced in cell culture and in vivo. *Methods Mol Biol* 2009;510:329–336.
30. Calattini S, Fusil F, Mancip J, Dao Thi VL, Granier C, Gadot N, Scoazec JY, Zeisel M, Baumert TF, Lavillette D, Dreux M, Cosset FL. Functional and biochemical characterization of HCV particles produced in a humanized liver mouse model. *J Biol Chem* 2015;290:23173–23187.
31. Vercauteren K, Van Den Eede N, Mesalam AA, Belouzard S, Catanese MT, Bankwitz D, Wong-Staal F, Cortese R, Dubuisson J, Rice CM, Pietschmann T, Leroux-Roels G, Nicosia A, Meuleman P. Successful anti-scavenger receptor class B type I (SR-BI) monoclonal antibody therapy in humanized mice after challenge with HCV variants with in vitro resistance to SR-BI-targeting agents. *Hepatology* 2014;60:1508–1518.
32. Maillard P, Walic M, Meuleman P, Roohvand F, Huby T, Le Goff W, Leroux-Roels G, Pecheur EI, Budkowska A. Lipoprotein lipase inhibits hepatitis C virus (HCV) infection by blocking virus cell entry. *PLoS One* 2011;6:e26637.
33. Ellis EC, Nauglers S, Parini P, Mork LM, Jorns C, Zemack H, Sandblom AL, Bjorkhem I, Ericzon BG, Wilson EM, Strom SC, Grompe M. Mice with chimeric livers are an improved model for human lipoprotein metabolism. *PLoS One* 2013;8:e78550.



34. Scholtes C, Ramiere C, Rainteau D, Perrin-Cocon L, Wolf C, Humbert L, Carreras M, Guironnet-Paquet A, Zoulim F, Bartenschlager R, Lotteau V, Andre P, Diaz O. High plasma level of nucleocapsid-free envelope glycoprotein-positive lipoproteins in hepatitis C patients. *Hepatology* 2012; 56:39–48.
35. Bukong TN, Momen-Heravi F, Kodys K, Bala S, Szabo G. Exosomes from hepatitis C infected patients transmit HCV infection and contain replication competent viral RNA in complex with Ago2-miR122-HSP90. *PLoS Pathog* 2014;10:e1004424.
36. Gastaminza P, Dryden KA, Boyd B, Wood MR, Law M, Yeager M, Chisari FV. Ultrastructural and biophysical characterization of hepatitis C virus particles produced in cell culture. *J Virol* 2010;84:10999–11009.
37. Meunier JC, Engle RE, Faulk K, Zhao M, Bartosch B, Alter H, Emerson SU, Cosset FL, Purcell RH, Bukh J. Evidence for cross-genotype neutralization of hepatitis C virus pseudo-particles and enhancement of infectivity by apolipoprotein C1. *Proc Natl Acad Sci U S A* 2005; 102:4560–4565.
38. Meunier JC, Russell RS, Engle RE, Faulk KN, Purcell RH, Emerson SU. Apolipoprotein c1 association with hepatitis C virus. *J Virol* 2008;82:9647–9656.
39. Felmlee DJ, Sheridan DA, Bridge SH, Nielsen SU, Milne RW, Packard CJ, Caslake MJ, McLauchlan J, Toms GL, Neely RD, Bassendine MF. Intravascular transfer contributes to postprandial increase in numbers of very-low-density hepatitis C virus particles. *Gastroenterology* 2010;139:1774–1783, 1783 e1–6.
40. Cahova M, Dankova H, Palenickova E, Papackova Z, Kazdova L. The opposite effects of high-sucrose and high-fat diet on fatty acid oxidation and very low density lipoprotein secretion in rat model of metabolic syndrome. *J Nutr Metab* 2012;2012:757205.
41. Nicholls SJ, Lincoff AM, Barter PJ, Brewer HB, Fox KA, Gibson CM, Grainger C, Menon V, Montalescot G, Rader D, Tall AR, McEneaney E, Riesmeyer J, Vangerow B, Ruotolo G, Weerakkody GJ, Nissen SE. Assessment of the clinical effects of cholesteryl ester transfer protein inhibition with evacetrapib in patients at high-risk for vascular outcomes: rationale and design of the ACCELERATE trial. *Am Heart J* 2015; 170:1061–1069.
42. Barter PJ, Rye KA. Cholesteryl ester transfer protein inhibition is not yet dead-pro. *Arterioscler Thromb Vasc Biol* 2016;36:439–441.
43. Maillard P, Krawczynski K, Nitkiewicz J, Bronnert C, Sidorkiewicz M, Gounon P, Dubuisson J, Faure G, Crainic R, Budkowska A. Nonenveloped nucleocapsids of hepatitis C virus in the serum of infected patients. *J Virol* 2001;75:8240–8250.
44. Piver E, Boyer A, Gaillard J, Bull A, Beaumont E, Roingard P, Meunier JC. Ultrastructural organisation of HCV from the bloodstream of infected patients revealed by electron microscopy after specific immunocapture. *Gut* 2017;66:1487–1495.
45. Saeed M, Andreo U, Chung HY, Espiritu C, Branch AD, Silva JM, Rice CM. SEC14L2 enables pan-genotype HCV replication in cell culture. *Nature* 2015;524:471–475.
46. Haas ME, Attie AD, Biddinger SB. The regulation of ApoB metabolism by insulin. *Trends Endocrinol Metab* 2013; 24:391–397.
47. Wang A, Huen SC, Luan HH, Yu S, Zhang C, Gallezot JD, Booth CJ, Medzhitov R. Opposing effects of fasting metabolism on tissue tolerance in bacterial and viral inflammation. *Cell* 2016;166:1512–1525 e12.
48. Bissig-Choisat B, Wang L, Legras X, Saha PK, Chen L, Bell P, Pankowicz FP, Hill MC, Barzi M, Leyton CK, Leung HC, Kruse RL, Himes RW, Goss JA, Wilson JM, Chan L, Lagor WR, Bissig KD. Development and rescue of human familial hypercholesterolaemia in a xenograft mouse model. *Nat Commun* 2015;6:7339.

---

Received November 22, 2016. Accepted July 10, 2017.

#### Correspondence

Address correspondence to: Ursula Andreo, PhD, Center for the Study of Hepatitis C, The Rockefeller University, 1230 York Avenue, Box 64, New York, New York 10065. e-mail: [uandreo@gmail.com](mailto:uandreo@gmail.com); fax: (212) 327-7048.

#### Acknowledgment

The authors thank Viet Loan Dao Thi for critical reading of the manuscript. The authors also wish to acknowledge Santa Maria Pecoraro Di Vittorio, Joseph Palarca, Glen Santiago, Julia Sable, Michael Pearce, Mary Ellen Castillo, Arnella Webson, and Sonia Shirley for outstanding administrative and/or technical support.

#### Author contributions

Ursula Andreo, Ype P. de Jong, Margaret A. Scull, and Charles M. Rice designed the study and analyzed data; Ursula Andreo, Ype P. de Jong, Jing W. Xiao, Koen Vercauteren, Corrine Quirk, Michiel C. Mommersteeg, Sonia Bergaya, and Arjun Menon performed experiments; Edward A. Fisher helped design the study and provided the fast-performance liquid chromatography equipment; Ursula Andreo, Ype P. de Jong, Koen Vercauteren, Margaret A. Scull, Edward A. Fisher, and Charles M. Rice edited the manuscript; and Ursula Andreo wrote the manuscript.

#### Conflicts of interest

The authors disclose no conflicts.

#### Funding

This work was supported by Office Director/National Institutes of Health/National Institute of Diabetes and Digestive and Kidney Diseases grants R01 DK085713 (C.M.R.) and K08 DK090576 (Y.P.J.), the National Institutes for Allergy and Infectious Diseases grant F32 AI091207 (M.A.S.), and the American Association for the Study of Liver Diseases Liver Scholar award (U.A.). The content is solely the responsibility of the authors and does not necessarily represent the official views of the National Institutes of Health or the American Association for the Study of Liver Diseases.